TECHNISCHE MECHANIK
an open access journal

Tech. Mech., Vol. 44, Is. 2, (2024), 100–109

Received: 08.07.2024
Accepted: 29.07.2024
Available online: 29.07.2024

journal homepage: www.ovgu.de/techmech

Development of a screw extruder for extracting linseed oil from flax

T. Krüger[1]* and S. Kirchhof[2]

[1] Technische Universität Bergakademie Freiberg, Institute of Mechanics and Fluiddynamics, Lampadiusstraße 4, 09599 Freiberg, Germany
[2] HTW Dresden - University of Applied Sciences, Faculty of Mechanical Engineering, Friedrich-List-Platz 1, 01069 Dresden, Germany

Abstract: Due to the short shelf life of linseed oil, it makes sense to produce it by pressing linseed directly before consumption. In order to gain knowledge about the pressing process, a simulation model using the Discrete Element Method (DEM) was created. For the description of the model basic tests were carried out to determine characteristic parameters of the seeds such as modulus of elasticity, coefficients of friction, particle size and bulk density. Subsequently an oil press has been designed and a prototype was produced. Experiments in which linseed, rapeseed and hemp has been processed under different test conditions have shown moderate functionality. As a result the mass flow in the entry section of the prototype was adjusted. Within this modification a modular structure was realized in order to enable further adaptations and tests with less effort.

Keywords: oil press, linseed, extruder, DEM, particle, bulk solids

1 Introduction

It is widely accepted that linseed oil got a positve effect on health, Al-Madhagy et al. (2023). The beneficial properties decrease if the oil is stored for too long or if it is manufactured incorrectly, Lu et al. (2019). Usually the oil needs to be compressed from linseed at low temperatures in a continuous process. A common method is to feed the material to be processed to a screw extruder. By rotation the seed is transported in axial direction, which is going along with a decrease of the enclosing volume. Consequently, the linseed is compressed and releases oil, which can be lead out of the machine via holes or slots either in the extruder shaft, which for this case needs to be a hollow shaft, or the surrounding shell. There are different possibilities to realize the decreasing volume. For established arrangements the outer diameter is preferred to be constant whereas the core diameter of the shaft increases. To avoid excessive pressure values, it is necessary to separate conveying and compression zones in each step of volume reduction, Schein (2003), Knuth and Homann (1980). For this purpose the helix is interrupted before the core diameter is increased. In this zone the compression is realized. The zone with helix and constant core diameter is referred to as the conveying area. The oil seeds will be referred to as particles. The principle is illustrated in figure 1.

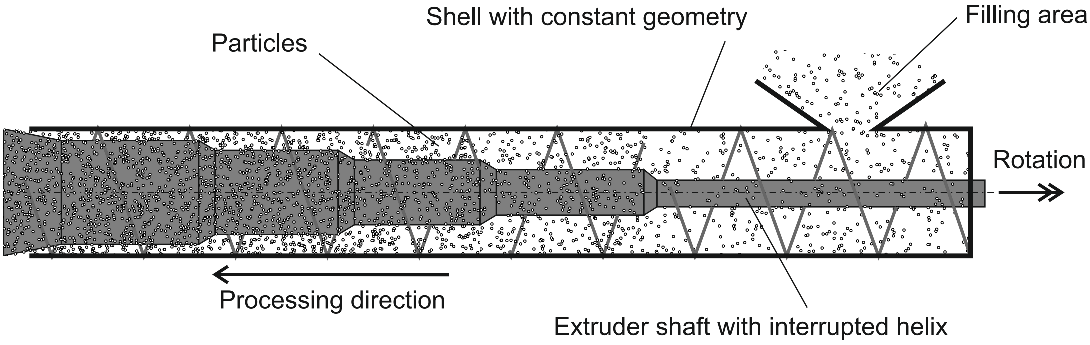

Fig. 1: Common design of a continuous working oil press with constant outer diameter und increasing shaft diameter

In order to achieve a better understanding of the process, a simulation using the Discrete Element Method (DEM) has been set up to model the process. Therefore several parameters need to be determined, such as mass, volume, density and shape of the particles. For the contact behavior it is necessary to identify Young's modulus and coefficients of friction. Established shear tests to analyze the friction between the particles among each other and the interaction between the particles and steel must be performed accordingly. Simulations with spherical particles improve basic understanding of the process, but also show the necessity to consider the shape of the particles, as the kinematic interaction of the particles is not well represented.
To validate and improve functionality, a prototype of the extruder was produced and different kinds of plant seeds were processed. Since the function was not satisfactory, modifications are necessary. To save costs, only the extruder shaft was altered, whereas the shell remained unchanged. As the drain of oil during the test was blocked significantly, the feed rate of the particles had to be reduced, achieved by enlarging the core diameter of the extruder shaft. To avoid producing unreasonable amounts of shafts and still being able to run more tests with different extruder geometries, the shaft was redesigned consisting of removeable helix elements. Expenses for further variations regarding the helix can be limited by only manufacturing the elements to be modified.

---

* E-mail address: thomas.krueger@imfd.tu-freiberg.de

doi: 10.24352/UB.OVGU-2024-058

2 Simulation of the pressing process

2.1 Parameter identification

For the simulation the following parameters need to be identified.

- Mass, volume, density, shape, inertia tensor of the particles and particle size distribution
- Young's Modulus of the particles
- Coefficient of friction for the interaction between the particles among each other – internal friction
- Coefficient of friction for the interaction between the particles and the machine parts – external friction

2.1.1 Mass properties and shape of the particles

To assess wether the linseed particles are subjected to a relevant statistical dispersion regarding its mass properties, a Computerized-Particle-Analysis-Device (CPA) was used to analyse the size and the shape of the particles. For this purpose the particles move over a vibrating chute and fall into a container. During the fall the particles are analysed by a camera, whereby the vibrations are adjusted in order to control the particle flow and to prevent the particles from overlapping. It turns out that size and shape of the particles, characterized by parameters such as sphericity (Zlatev (2005)) and equivalent diameter do not scatter significantly. The cumulative distribution functions of all examined parameters show a strong increase to 100 % at a certain value. Since it is assumed that mass properties correlate strongly with size and shape, it is very useful to calculate average values accordingly and use them without dispersion in the simulation.
As it is difficult to get the mass m_p of very light linseed particle by weighing it, the mass is obtained by determining the quantity of 3 g particles. This results in a particle mass of $m_\mathrm{p} = 6.4 \cdot 10^{-6}\,\mathrm{kg}$. The density ρ_p is derived by filling 100 g of particles together with water into a container of the defined volume $V_\mathrm{G} = V_\mathrm{W} + V_\mathrm{P100}$, where V_W and V_P100 refer to the volumes of water and the particles accordingly. As the volumes can be calculated from corresponding density and mass, the required density ρ_p derives from

$$\frac{m_\mathrm{P100}}{\rho_\mathrm{p}} + \frac{m_\mathrm{W}}{\rho_\mathrm{W}} = V_\mathrm{G}, \tag{1}$$

where m_P100, m_W, ρ_W and V_G are known parameters. The density results in $\rho_\mathrm{p} = 1057\,\frac{\mathrm{kg}}{\mathrm{m}^3}$. Considering the mass $m_\mathrm{p} = 6.4 \cdot 10^{-6}\,\mathrm{kg}$ the volume of a single particle is $V_\mathrm{p} = 6.05 \cdot 10^{-9}\,\mathrm{m}^3$. For the simulation in the DEM software environment Liggghts DSC (2024) there are different possibilities to assign mass properties to a particle. One can specify geometric parameters and density that result in properties like mass and inertia tensor internally. It is also possible to specify the mass and the inertia tensor directly. To obtain the inertia tensor of a single linseed particle, a mathematical description of the surface is required. Subsequently, and by assuming a homogeneous density, the inertia tensor can be calculated. As contact-based and standard scanning procedures fail due to the small size and the low strength, photos of a single particle were analyzed. Images, which show projections of a particle on three orthogonal coordinate planes, have been used to redraw the contour of the projections. The resulting splines were interpolated to form a 3D model, see figure 2.

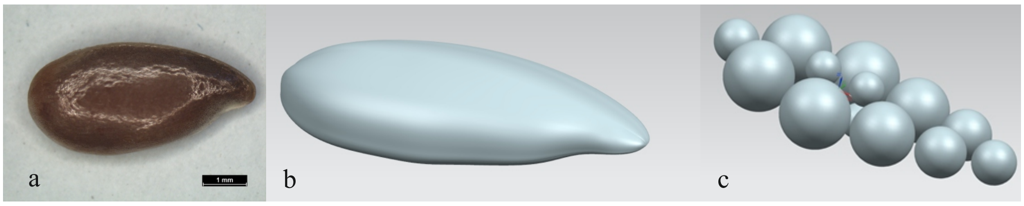

Fig. 2: Linseed particle designed in CAD (b) based on photographs (a) and a multisphere particle (c) Lange et al. (2019)

With the constant density $\rho_\mathrm{p} = 1057\,\frac{\mathrm{kg}}{\mathrm{m}^3}$ the inertia tensor is

$$\mathbf{I}_\mathrm{P} = \begin{bmatrix} 0.231 & 0.003 & 0.009 \\ 0.003 & 0.783 & -0.015 \\ 0.009 & -0.015 & 0.927 \end{bmatrix} 10^{-11}\,\mathrm{kg} \cdot \mathrm{m}^2. \tag{2}$$

Using spherical particles in the simulation, the equivalent radius r_p is derived from the volume V_p as $r_\mathrm{p} = 1.13\,\mathrm{mm}$. For further simulations the linseed can be recreated by multishpere particles. These particles consists of spheres that are rigidly connected to each other. For the linseed 15 spheres of different sizes were arranged in such a way that the shape of the linseed is represented appropriately, see figure 2. Noting that increasing the number of spheres extends the calculation time.

2.1.2 Young's modulus of the particles

Elastic contact in the normal direction according to Hertz is assumed for the simulation. Two materials, steel and linseed, appear to make contact with each other. The modulus of elasticity of steel is $E_\mathrm{s} = 2.1 \cdot 10^{11}\,\frac{\mathrm{N}}{\mathrm{m}^2}$. The deformation behavior of the linseed particles can only be investigated in a compression test, as for tensile testing the particles cannot be fixed properly. For this purpose a universal testing machine was used. As the particles are natural products, 20 particles were tested successively. The determined force-displacement-behavior is illustrated in figure 3.

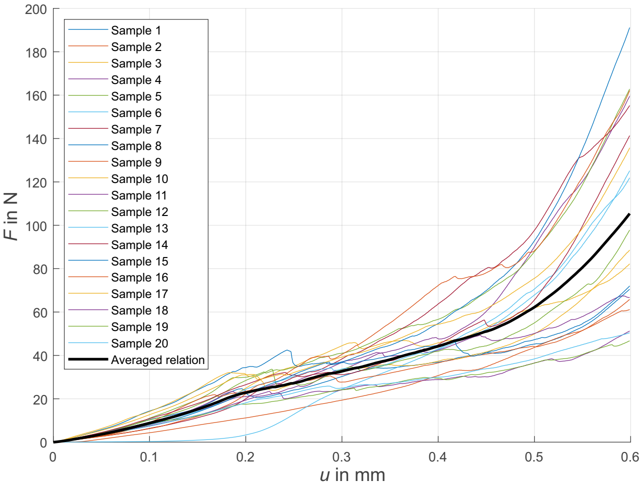

Fig. 3: Force-displacement behavior determined for 20 single linseed particles by compression testing

The approach to obtain the elastic modulus E_p of the particles is to simulate the test for several times while varying the parameter. This requires a corresponding start parameter. The relation between force F and displacement u is given in DSC (2024). The relation depends on different parameters and can be simplified by considering the existing test conditions. For the pairing of steel and linseed one can assume that the elastic modulus of steel is much larger than the one of the particles, $E_\mathrm{s} \gg E_\mathrm{p}$. Furthermore each particle is pressed between two plates, i. e. the radius of each plate r_s is infinite. Eventually, the measured displacement is twice the overlap between the contact partners described in DSC (2024), as the overlapping occurs on both sides of the particle. From that and according to Hertz theory the relation

$$F = \frac{4}{3}\cdot\sqrt{\frac{r_\mathrm{p}}{8}}\cdot\frac{E_\mathrm{p}}{1-\nu_\mathrm{p}^2}\cdot u^{\frac{3}{2}} \tag{3}$$

can be found, which includes the Poisson's ratio of the particles $\nu_\mathrm{p} = 0.3$, Horabik and Molenda (2016). There are 600 datapoints available for F and u, which form the averaged curve in figure 3. Applying the Residual sum of squares method in order to fit equation 3 to the measurings, the parameter E_p^* can be determined by

$$E_\mathrm{p}^* = \frac{6\,(1-\nu_\mathrm{p}^2)\,\sum_k^{600} F_k\cdot u_k^{\frac{3}{2}}}{\sqrt{8\,r_\mathrm{p}}\,\sum_k^{600} u_k^3} = 348.8\,\mathrm{MPa}. \tag{4}$$

This means that a sphere with the elastic modulus $E_\mathrm{p}^* = 348.8\,\mathrm{MPa}$ and the radius $r_\mathrm{p} = 1.13\,\mathrm{mm}$, which is compressed like the linseed particles in the experiments, exhibits a deformation behavior that fits the measured curves in terms of the sum of squared residuals. As the linseed particles were compressed lying on their flat side, it is to be expected that a smaller value for E_p leads to the measured behavior. Several simulations of the compression test by lowering the parameter E_p and using the multisphere particle shown in figure 2c were performed. The deformation behavior is compared to the averaged curve in figure 3 using the sum of squared residuals, which leads to a value of $E_\mathrm{p} = 200\,\mathrm{MPa}$. The best fit is shown in figure 4.

2.1.3 Internal friction

Bulk solids, in general, can neither be described as fluids nor as deformable solids. They appear as an intermediate category in which interactions occur between the particles Hinterreiter (2010). In this context the internal friction among the particles can be considered statically and dynamically Schulze (2014). Furthermore, dynamic friction processes must be differentiated as stationary or transient. Since the stationary process is to be simulated, the stationary coefficient $\mu_\text{p-p,s}$ of friction is required accordingly. A simple approach is to heap up the material in a defined manner and measure the angle of repose. The test and its conditions for implementation are standardized in e. g. DIN ISO 4324 and DIN 1055-1 and lead to a static coefficient. According to Scheffler (1980) the dynamic coefficient is 0.7 times lower than the coefficient identified by the angle of repose. The heaped linseed forms an angle of 35 °, which leads to $\mu_\text{p-p,s} = 0.7 \cdot \tan 35° = 0.49$ as a first guess. A more precise approach is to use a ring shear device, an established test rig to identify the stationary coefficient of friction. The operating principle is sufficiently described in the literature, e. g. in Schulze (2014), Rakitsch (2012), Hinterreiter (2010), Scheffler (1980). Figure 5 shows a basic sketch to explain the working principle.

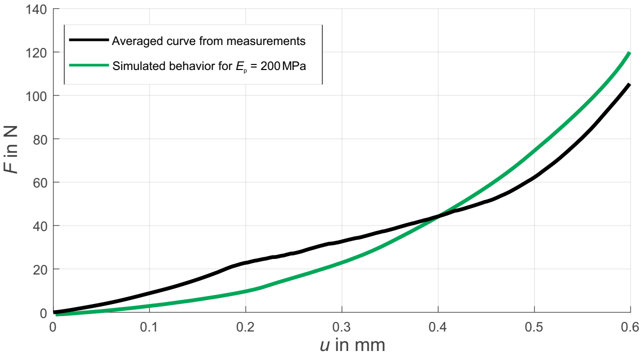

Fig. 4: Averaged force-displacement behavior of linseed particles and multisphere particles with $E_\mathrm{p} = 200\,\mathrm{MPa}$

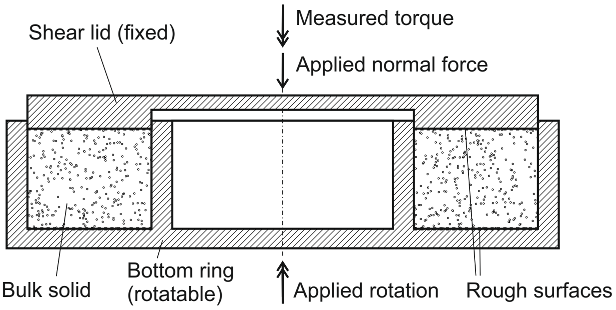

Fig. 5: Working principle of a ring shear test

The particles are filled into a bottom ring and are covered by a shear lid, which is loaded by a normal force. To prevent sliding between the bulk material and the bottom or the lid, the according surfaces have a rough finish. The bottom ring performs a rotational movement, while the enclosed particles transmit a torque to the lid. Thus, the internal friction properties can be deduced from the measured torque. With the beginning of the rotation the particles start to consolidate going along with an increasing torque. At a certain point there is no further solidification and a relative motion among the particles results in a decreasing torque. A steady state is reached when the torque remains constant. Under that condition the ratio between averaged values of shear and normal stress lead to the stationary coefficient of friction $\mu_{\mathrm{p\text{-}p,s}} = 0.52$. This value is chosen for the simulation, since the parameter is identified during a stationary movement directly. The deviation from the initially encountered value of 0.49 is acceptable.

2.1.4 External friction

Essentially the particles are in contact with the extruder shaft during the pressing process. The shaft is made of steel and primarily manufactured by milling. With this method values between 1.6 µm and 12.5 µm can be achieved for the surface roughness parameter R_a (Arithmetic Average of Roughness Profile), Falk et al. (2005). As low roughness values are to be aimed for the shaft, two steel plates with roughnesses 1.6 µm and 3.2 µm are produced in order to investigate the friction behavior accordingly.
An obvious method is to let single particles slide down an inclined plane on which the plates are mounted. The slope angle, which causes the particle to move with constant velocity, leads to the sliding coefficient of friction. The feasibility shows difficulties because the particle starts to move, when the slope angle exceeds the angle of static friction, which is normally larger than the one for sliding friction. At this moment the angle must be reduced to stop the acceleration of the particle. This approach therefore usually leads to friction values that are to high. At least upper limits for the friction coefficients $\mu_{\mathrm{p\text{-}s,1.6}} = 0.55$ and $\mu_{\mathrm{p\text{-}s,3.2}} = 0.76$ were determined for the two plates. Eventually, the parameters were identified performing a translational shear test by a Jenike shear cell which is shown in figure 6.

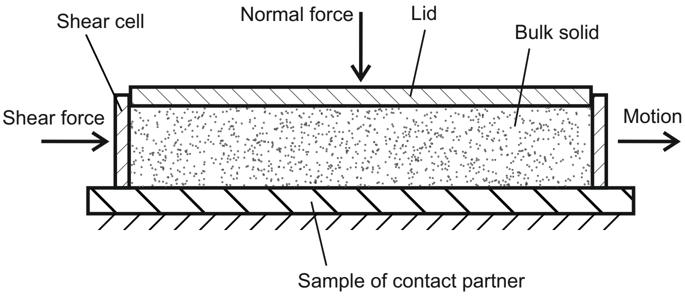

Fig. 6: Working principle of the Jenike shear cell

The cell is placed on the fixed sample plate. The linseeds are filled into the device and are covered by a lid that is loaded by a normal force. A shear force is applied in such a way that the cell moves with constant velocity. The shear force corresponds to the

frictional force and the coefficient of friction can be determined from the ratio of shear and normal force, Hinterreiter (2010), Schulze (2014). The sliding friction parameters are $\mu_{\text{p-s},1.6} = 0.22$ and $\mu_{\text{p-s},3.2} = 0.24$ for the surfaces with roughnesses 1.6 µm and 3.2 µm. As expected, the resulting values are smaller than the previously identified upper limits. In the simulation the parameter $\mu_{\text{p-s}} = 0.22$ is used to model the friction between the particles and the extruder shaft.
Besides the shaft the particles are in contact with the fixed shell surrounding the compression volume. Due to obvious reasons one needs to achieve that the particles which are in contact with the inner surface, don't move relative to the shell in circumferential direction. This ensures the particles to be conveyed in processing direction. The inner surface was deliberately designed to be rough, Meskat (1962), so for first simulations the external friction between the shell and the bulk solid is not investigated and the relative movement is blocked in the model.

2.2 Simulation with spherical particles

Since the simulation using multisphere particles requires a huge amount of computing time, initially it is set up with spherical particles, see figure 7a. On the one hand the simulation illustrates the tracing of the particles during the process. On the other hand the loading of the shaft and the shell can be calculated in order to perform stress analyses using the Finite Element Method (FEM) on these components. Within the simulation the geometries are integrated as stl-files which represent the bodies as triangulated surfaces. For each triangle a cartesian force vector as a reaction of the particle movement is calculated. Since the coordinates of each triangle vertexes are known, the according surface area and the normal unit vector lead to a stress vector that can be separated into normal and tangential components. Each component can be further split into circumferential, radial and axial directions depending on the circumferential position of the point of origin of the vector. The loads formulated in this way are suitable to be implemented in FEM software. Noting that the separation in normal and tangential stresses is not necessary, but helps verifying the results.

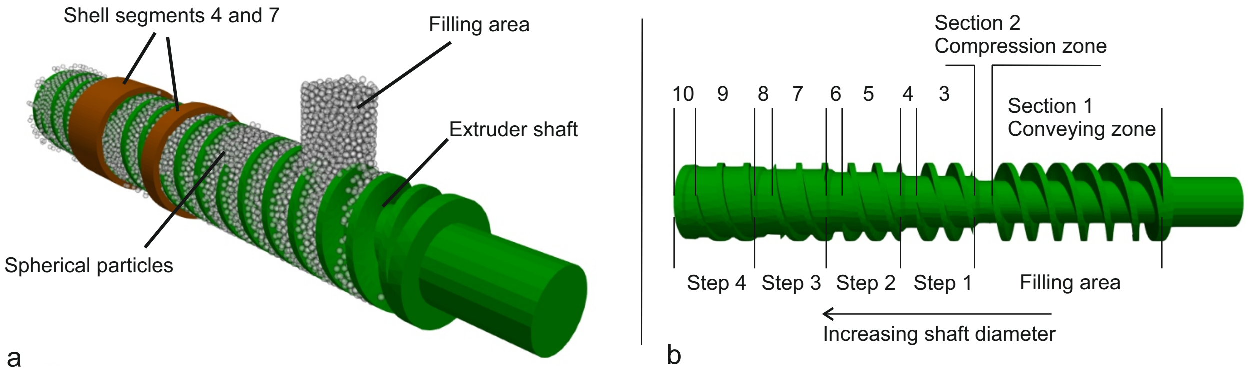

Fig. 7: a) Simulation of continuous pressing process with the shell suppressed, apart from segments 4 and 7, b) Partitioning of the pressing volume based on the geometry of the shaft

Since similar stress values are expected within the different stages of the process, shaft and shell are devided into 10 sections, see figure 7b. The shell segments, e. g. segments 4 and 7 see figure 7a, don't need to be subdivided any further, whereas the shaft surface and the two helixes with its front and rear side must be considered separately, see figure 8a. The loads calculated with DEM for each triangle are averaged for the described sections. Figure 8b shows the extracted normal stress of 57 kPa acting on the front surface of the helixes in section 7.

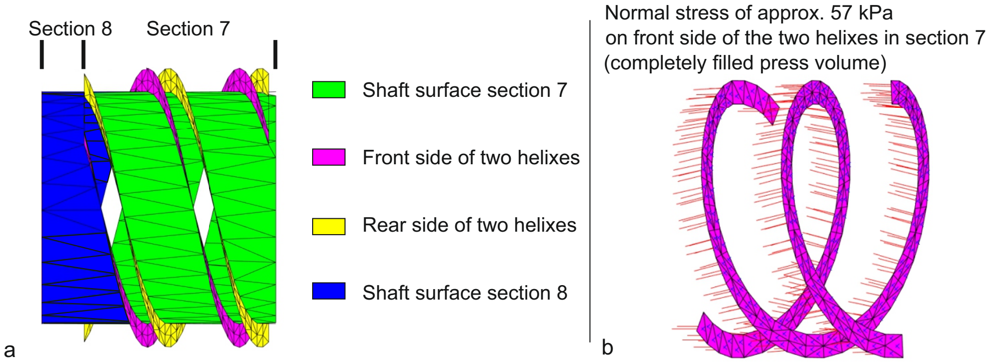

Fig. 8: Partitioning of the shaft surface and normal stress on the front side of the two helixes

As the simulation with spherical particles is used to test the implementation, at this stage of the project the numeric results are less important. Nevertheless, it is noticeable that the calculated stress values are quite small in general. This is most likely related to the shape of the particles (Hofmann (2013)), as spheres don't interact like the linseed particles shown in figure 2. Spheres tend to roll on the surfaces of the involved contact partners, like shaft, shell and the other particles. Although it is still open to verify by simulations with multisphere particles, this leads to the behavior shown in figure 9 for the filling phase. The rolling motion among the spheres favors the particles to circle together with the shaft while poor forward movement is observed. Since the inner surface of the shell is very rough, the circling motion is expected to be more limited by using multisphere particles going along with an increasing movement in processing direction. In the simulation the minor forward movement stops completely as soon as the press volume is filled. An improved axial movement by using multisphere particles may lead to a continuous flow of particles, as the higher pressure caused by the increased number of particles forces them to exit the press in processing direction.

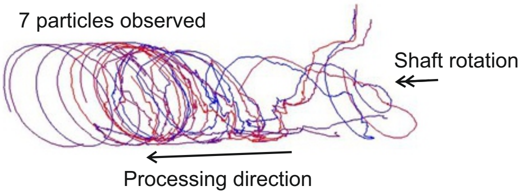

Fig. 9: Observation of the trajectories of the movement of 7 particles during the filling procedure

The upcoming work regarding the simulation involves primarily two points. The simulation is to be carried out with multisphere particles using the geometry shown in figure 2 as well as mass and inertia tensor determined in section 2.1.1. Then a suitable force criterion must be identified in order to simulate the oil release. In this context the according mass and volume reduction of a particle needs to be identified and implemented in the simulation.

3 Prototype of the oil press

In order to test the functionality of the oil press, a prototype was manufactured. As the results proved to be unsatisfactory, the mass flow during the process was reconsidered to adapt the shaft core diameter. Based on this a new design is suggested. It uses removeable helix elements to allow further variations with little effort.

3.1 Basic features and pressing tests

The shaft, including two interrupted helixes, and the shell are the components of the oil press that influence the process essentially. The according CAD models of the prototype are shown in figure 10.

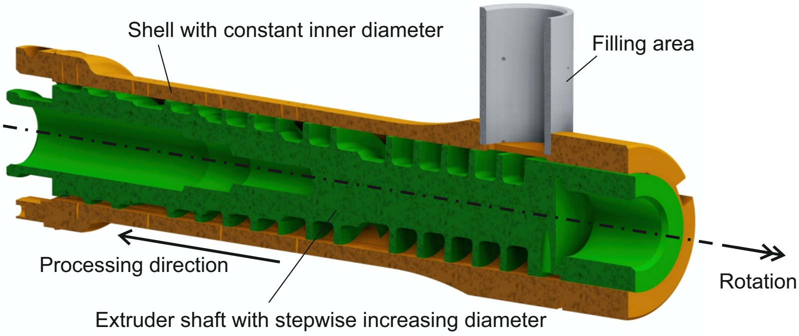

Fig. 10: CAD section view of shaft with two helixes and shell

For the prototype a simple target of an oil production of 50 ml per minute is set. This means an oil mass flow of $7.75 \cdot 10^{-4}\,\frac{\mathrm{kg}}{\mathrm{s}}$ as the density of the oil is given by $930\,\frac{\mathrm{kg}}{\mathrm{m}^3}$. The ratio of oil and linseed mass is approx. 0.365, BLS (2024), resulting in a linseed mass flow of $\dot{m}_{\mathrm{LS}} = 2.12 \cdot 10^{-3}\,\frac{\mathrm{kg}}{\mathrm{s}}$. As the mass flow is calculated from

$$\dot{m}_{\mathrm{LS}} = \rho_{\mathrm{LS}} \cdot A_{\mathrm{PVi}} \cdot n_{\mathrm{S}} \cdot h_{\mathrm{H}}, \tag{5}$$

including the measured bulk density of linseed $\rho_{\mathrm{LS}} = 613\,\frac{\mathrm{kg}}{\mathrm{m}^3}$, the rotation speed of the shaft $n_{\mathrm{S}} = 13\ \mathrm{min}^{-1}$ and the pitch of one helix $h_{\mathrm{H}} = 26\,\mathrm{mm}$, a cross section area $A_{\mathrm{PVi}} = 614.87\,\mathrm{mm}^2$ of the initial press volume is derived by equation 5. The value leads to the diameter of the shaft d_{S} where the particles are filled in.
Considering figure 11 the relations

$$A_{\mathrm{PVi}} = \frac{\pi}{4}\left(D_{\mathrm{S}}^2 - d_{\mathrm{S}}^2\right) - t \cdot \left(D_{\mathrm{H}} - d_{\mathrm{S}}\right), \tag{6}$$

$$s = t \cdot \sin\alpha, \tag{7}$$

$$\tan\alpha = \frac{2\,h_{\mathrm{H}}}{\pi\left(D_{\mathrm{H}} + d_{\mathrm{S}}\right)} \tag{8}$$

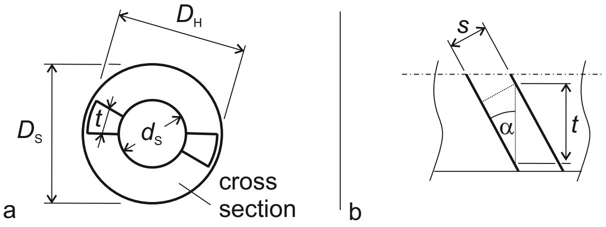

Fig. 11: Parameters to calculate the cross section area A_{PVi} of the press volume, a) cross section of shaft with helixes and shell, b) inclined helix with wall thickness s

are obtained. Since $\tan\alpha \approx \sin\alpha$ and $D_{\mathrm{H}} = 39.4\,\mathrm{mm} \approx D_{\mathrm{S}} = 39.7\,\mathrm{mm}$ can be assumed, equations 6 to 8 lead to

$$A_{\mathrm{PVi}} = \pi \left(\frac{1}{4} - \frac{s}{2\,h_{\mathrm{H}}}\right) \left(D_{\mathrm{S}}^2 - d_{\mathrm{S}}^2\right). \tag{9}$$

With $s = 3\,\mathrm{mm}$ and $D_{\mathrm{S}} = 39.7\,\mathrm{mm}$ the diameter $d_{\mathrm{S}} = 23.6\,\mathrm{mm}$ is derived. For the compression steps in processing direction, the diameters were increased evenly.

Based on the considerations described the prototype was produced and tested. Three types of plant seeds, linseed, rapeseed and hemp, were processed at different experimental conditions respectively. On the one hand the rotation speed was varied from 13 to 22 min^{-1}. On the other hand the shaft and the shell were heated to 50 °C in additional tests. The variations intend to show dependencies, but neither the fast rotation, as it benefits increased temperatures, nor the directly induced heat are desired conditions. The tests ran not satisfactory for the different seeds with the observed weaknesses proving to be very similar. The material was conveyed as expected and oil mixed with solid leaked from the holes in the shell in processing areas 9 and 10, compare figure 7. It turns out that the holes are too large to retain the solids. This lack of functionality is less significant, whereas all tests need to be canceled due to blocked material transport. An accumulation of pressed material appeared in sections 7 to 10 of the compression volume, see figure 12a.

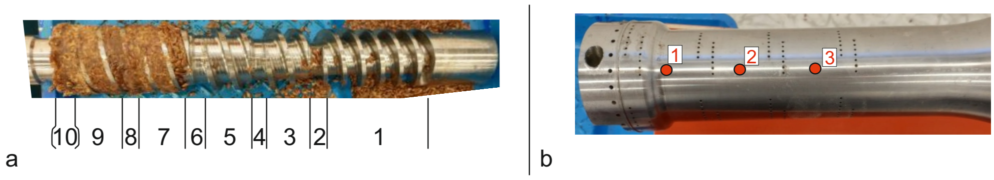

Fig. 12: a) Accumulation of compressed linseed on disassembled shaft, b) Measuring points on the shell to determine the temperature

An increase in speed has basically no influence on this behavior, except that the displayed state is reached more quickly. In order to observe heat generation, the temperatures were measured at different points of the shell, see figure 12b. During the tests that started at 20 °C, a rise of temperatures was detected, especially at regions exposed to high pressures. At measuring points 1, 2 and 3 the temperature rose by approx. 15 K, 10 K and ≈ 0 K respectively using a rotation speed of 22 min^{-1}. The test performed with speed of 13 min^{-1} caused less heat production. At point 1 a rise of approx. 5 K was measured. This affirms the correctness of using a low rotation speed for the procedure. Heating the shaft and the shell to 50 °C doesn't lead to improvements regarding the pressing behavior. The temperature remained unchanged during the test.

Since the blockage of the oil press is most likely caused by an excessive supply of material to the sections of low press volume, the rate of the volume reduction shall be decreased accordingly. To keep the effort low, the shell geometry is not changed. Instead, the core diameter of the shaft is increased in the filling area, resulting in less material to be processed and a lower rate of compression.

3.2 Reducing the compression volume

To adapt the shaft diameter suitably, the bulk density of $\rho_{\mathrm{LS}} = 613\,\frac{\mathrm{kg}}{\mathrm{m}^3}$ as well as the density of the compressed material $\rho_{\mathrm{LSp}} = 1.17 \cdot 10^3\,\frac{\mathrm{kg}}{\mathrm{m}^3}$, excluding the oil, has been taken into account. Both parameters were identified via weighing a defined volume. Since equation 5 refers to the filling area the relation

$$\dot{m}_{\mathrm{LSp}} = \rho_{\mathrm{LSp}} \cdot A_{\mathrm{PVe}} \cdot n_{\mathrm{S}} \cdot h_{\mathrm{H}} \tag{10}$$

derives the mass flow at the output of the oil press. The inner diameter of the shell $D_{\mathrm{S}} = 39.7\,\mathrm{mm}$ and the retained final shaft diameter $D_{\mathrm{e}} = 37.4\,\mathrm{mm}$ lead to $A_{\mathrm{PVe}} = 139.27\,\mathrm{mm}^2$ and to $\dot{m}_{\mathrm{LSp}} = 9.18 \cdot 10^{-4}\,\frac{\mathrm{kg}}{\mathrm{s}}$ eventually. Considering the ratio of oil and linseed mass of 0.365, the mass flow of the bulk material in equation 5 equals $1.45 \cdot 10^{-3}\,\frac{\mathrm{kg}}{\mathrm{s}}$ and thus, the modified cross section area $A_{\mathrm{PVi}} = 418.62\,\mathrm{mm}^2$ for section 1 is obtained. Equation 9 results in the diameter $d_{\mathrm{S}} = 29.7\,\mathrm{mm}$ of the shaft in the filling area. Figure 13 illustrates the reduced compression rate. For the existing screw shaft the cross section area of the press volume decreases from 614.87 mm^2 to 139.27 mm^2, whereas for the modified shaft only 418.62 mm^2 are available to fill in material. The designations for the sections that have been introduced in figure 7 are marked in figure 13. The according compression zones are characterized by a sudden increase of the cross section area, caused by the interrupted helix.

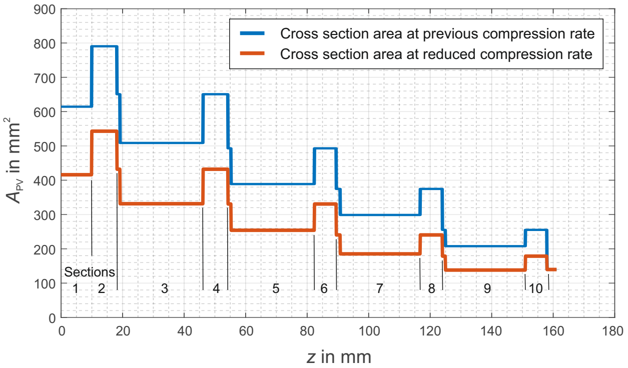

Fig. 13: Reduction of the rate of compression by reducing the cross section area of the press volume in the filling area

3.3 Modular extruder shaft

To consider the modifications and to keep the effort for further adaptations low, a modular assembled shaft consisting of 5 different helix elements was designed, see figure 14. The segments 1 to 5 got an increasing outer diameter and are connected to a shaft by a polygonal shaft-to-hub connection. Taking the available drive torque of $T_\text{t} = 186\,\text{Nm}$ as a basis, an equivalent diameter of $D_\text{M} = 18\,\text{mm}$ is chosen for the connection, INKOMA-Group (2014).

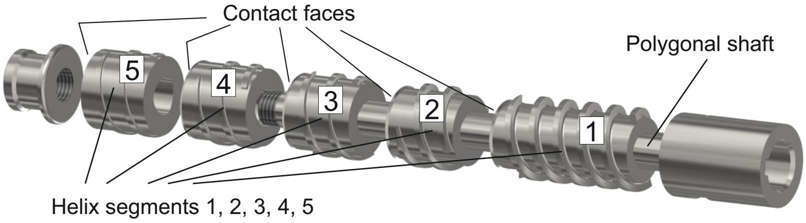

Fig. 14: Modular designed extruder shaft

Within a strength analysis done for the segments, two different kinds of loads are considered. First, an inner pressure p_i acts on the hub due to the torque transmission from the shaft, calculated by

$$p_i = \frac{T_\text{t}}{l_i\left(0.75 \cdot \pi \cdot D_\text{M} \cdot e + \frac{D_\text{M}^2}{20}\right)}, \tag{11}$$

where l_i is the length of the according segment and $e = 0.56\,\text{mm}$ a geometric parameter of the polygon, INKOMA-Group (2014). Arithmetically, the inner pressures are $p_1 = 63.8\,\frac{\text{N}}{\text{mm}^2}$, $p_2 = 133.0\,\frac{\text{N}}{\text{mm}^2}$, $p_3 = 133.0\,\frac{\text{N}}{\text{mm}^2}$, $p_4 = 133.8\,\frac{\text{N}}{\text{mm}^2}$ and $p_5 = 136.9\,\frac{\text{N}}{\text{mm}^2}$, even though the load at the segments 1, 2 and 3 is assumed to be low, caused by negligible transmission of torque resulting from nearly unpressed particles in these areas.
The second load to be considered also results from the torque $T_\text{t} = 186\,\text{Nm}$. It is assumed that it is caused by evenly distributed forces acting on the cylindrical surface of the segments in circumferential direction. Depending on radius and area, the tangentially acting loads τ_i are given by $\tau_1 = 2.7\,\frac{\text{N}}{\text{mm}^2}$, $\tau_2 = 4.1\,\frac{\text{N}}{\text{mm}^2}$, $\tau_3 = 3.6\,\frac{\text{N}}{\text{mm}^2}$, $\tau_4 = 3.4\,\frac{\text{N}}{\text{mm}^2}$ and $\tau_5 = 3.3\,\frac{\text{N}}{\text{mm}^2}$. Figure 15 summarizes the loads and the necessary boundary condition.

Furthermore, an axial load acts in different ways on the segments, Eggers et al. (1985). For the fifth segment forces are mainly initialized at the front side of the helix, whereas no force acts on the circular contact face of the segment, see figures 14 and 15. This ratio is gradually reversed for the fourth, third, second and first segment. The second segment transmits the axial force to the first via the contact surface and nearly no axial force acts on the helix since the material is not compressed at this stage of the process. Depending on the particle properties, pressure values of up to 15 $\frac{\text{N}}{\text{mm}^2}$ occur during the compression, Schein (2003), Ellermann et al. (1990). The value is assumed to act on the helix of the fifth segment. Since the area of the front side of one helix is quite small, the resulting axial force is quite low as well. Therefore, this effect is neglected, which goes along with the requirement that all surfaces in conveying direction shall be designed to be smooth. Note, the pressure inside the processing volume also acts radially. As for cylindrically shaped shells the radial external pressure counteracts the internal one, it is disregarded in the sense of a conservative approach.
The assumptions described lead to stresses which are mainly caused by the inner pressure. The tangential load got a minor

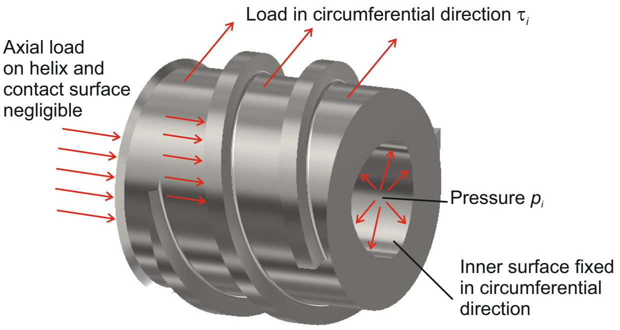

Fig. 15: Boundary conditions and orientation of loads for stress calculation

influence. The least critical stresses occur at segment 1, caused by a low inner pressure that results from the length of the segment, see equation 11. Since the other segments got almost same lengths, the small wall thickness of segment 2 leads to considerable stresses in this component.

Figure 16 illustrates the von Mises equivalent stress σ_v, the radial stress σ_rr and the circumferential stress σ_pp due to tangential load τ_2 and inner pressure p_2 for the second segment. The corresponding value at the most critical area, the contact surface to the polygonal shaft, is given. The von Mises stress σ_v, which is decisive for evaluation, results in 320 MPa. The amount originating from the tangential load is negligible. As there is no axial load considered, this value is largely composed of the radial stress $\sigma_\text{rr} = -140$ MPa and the circumferential stress $\sigma_\text{pp} = 240$ MPa. As expected for cylindrical shaped elements, the tension in circumferential direction is more significant. Furthermore, essential values occur where the helixes begin and end. These points should be designed with an appropriate radius.

For shaft-to-hub connections INKOMA-Group (2014) recommends tempered steel C45 with a yield strength of 430 MPa, Falk et al. (2005). Since the von Mises equivalent stress σ_v is lower, the proof of strength under static conditions is verified for the modified oil press, especially when taking into account that the inner pressure at the second segment does not reach the value of $p_2 = 133.0\,\frac{\text{N}}{\text{mm}^2}$. It derives from the conservative assumption of full torque transmission at this stage of the process. Fatigue strength must not be taken into account because of the small amount of load cycles which have to be expected during the test of the modified prototype.

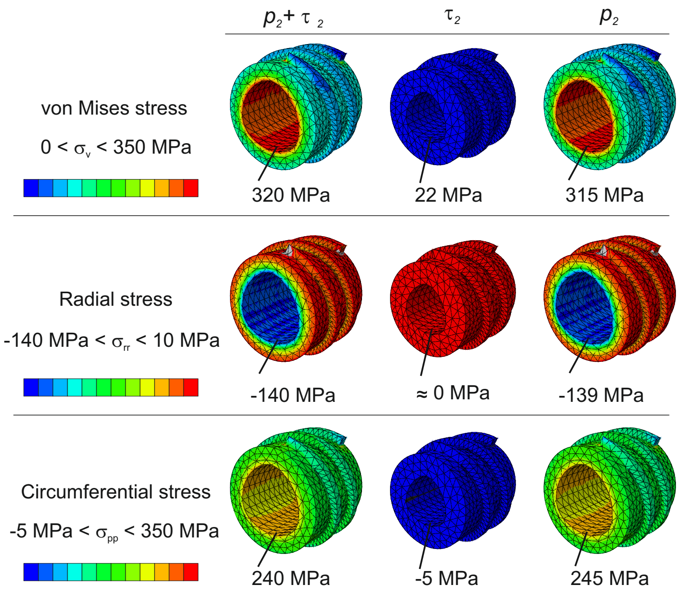

Fig. 16: Von Mises equivalent stress σ_v, radial stress σ_rr, circumferential stress σ_pp due to tangential load τ_2 and inner pressure p_2 at segment 2

4 Outlook

The designed prototype of an oil press was tested and showed functional deficiencies. On the one hand, in addition to oil many solids were extracted due to the boreholes that are too large to separate the solid from the liquid. While this is accepted for now, on the other hand the axial transport of particles stopped due to excessive amount of particles feeded to the process. To improve the flow of particles, the feeding is limited by reducing the press volume in the filling area. The modified oil press was designed modularly, allowing different shaft geometries to be tested with little effort. For a geometry adapted to the mass flow, a strength analysis was performed successfully. Eventually, a new shaft and helix elements, joined by a polygonal shaft-to-hub-connection, must now be manufactured to enable new tests that shall show improved functionality. A further step is to redesign the boreholes in order to improve the oil extraction.

The functional tests were preceded by simulations using the Discrete Element Method (DEM). For the modeling different experiments were carried out to identify system parameters as mass characteristics, Young's modulus and friction coefficients. In addition to the visualization of the particle flow the simulation calculates input data for further analyses such as load values in order to perform strength analyses. Since the simulation is basically working, it can be extended accordingly. One extension means the use of multisphere particles, which is required to reproduce the way the particles interact among each other. Necessarily, the increase of the density during the process from 613 $\frac{\mathrm{kg}}{\mathrm{m}^3}$ to 1170 $\frac{\mathrm{kg}}{\mathrm{m}^3}$ must be considered and implemented, going along with a reduction of mass due to the oil release. Experimental preparatory work needs to be done, including the identification of suitable force values that initiate the oil flow from the particles.

References

S. Al-Madhagy, N. S. Ashmawy, A. Mamdouh, O. A. Eldahshan, and M. A. Farag. A comprehensive review of the health benefits of flaxseed oil in relation to its chemical composition and comparison with other omega-3-rich oils. *European Journal of Medical Research*, 28, 2023.

BLS. German Nutrient Data Base. BLS-Version 3.02. https://www.blsdb.de/, February 2024.

DIN 1055-1. *Einwirkung auf Tragwerke- Teil 1: Wichten und Flächenlasten von Baustoffen, Bauteilen und Lagerstoffen*.

DIN ISO 4324. *Tenside, Pulver und Granulate, Bestimmung des Schüttwinkels*.

DSC. *Liggghts-Public Online Documentation*. DCS Computing GmbH, Linz, Austria, February 2024.

R. Eggers, H. Boeck, and W. Stein. Messung von Druck- und Temperaturprofilen beim Abpressen von Ölsaaten in Seiher-Schneckenpressen. *Fette Seifen Anstrichmittel*, 87:494–499, 1985.

I. Ellermann, D. Baumgart, H. Relitz, P. Specht, and G. Pocher. Anordnung zur Messung des radialen Drucks in Seiher-Schneckenpressen. Deutsches Patentamt, Offenlegungsschrift, 1990. DE 38 44 462 A1 vom 22.02.1990.

D. Falk, P. Krause, and G. Tiedt. *Metalltechnik Tabellen*. Westermann, 2005.

S. Hinterreiter. *Bestimmung und Einflussgrößen der Brückenbildung bei der Lagerentnahme von biogenen Festbrennstoffen*. Dissertation, Technische Universität München, 2010.

T. Hofmann. *Kinematikstudie sphärischer Partikel mithilfe der Diskreten Elemente Methode*. Masterarbeit, Technische Universität Bergakademie Freiberg, 2013.

J. Horabik and M. Molenda. Parameters and contact models for DEM simulations of agricultural granular materials: A review. *Biosystems Engineering*, 147:206–225, 2016.

INKOMA-Group. *Drive-Technology Welle-Nabe-Verbindungen*. INKOMA-Group, 38162 Schandelah, 2014.

M. Knuth and T. Homann. Fried. Krupp GmbH. Verfahren und Vorrichtung zur Ölgewinnung aus gereinigten Ölfrüchten und Ölsaaten. Deutsches Patentamt, Offenlegungsschrift, 1980. 29 15 538 vom 23.10.1980.

N. Lange, R. Schirmer, and A. Hasche. *Untersuchungen und Simulationen zum Ölpressen aus Leinsamen*. Projektarbeit, Technische Universität Bergakademie Freiberg, 2019.

T. Lu, Y. Shen, J.-H. Wang, H.-K. Xie, Y.-F. Wang, Q. Zhao, D.-Y. Zhou, and F. Shahidi. Improving oxidative stability of flaxseed oil with a mixture of antioxidants. *Journal of Food Processing and Preservation*, 44, 2019.

W. Meskat. Der Fliess- und Entlaugungsvorgang einer Alkalicellulosefaser-Suspension in einer Schneckenpresse. *Chem.-Ing.-Techn.*, 34:742–748, 1962.

S. Rakitsch. *Dimensionierung und Auslegung stark geneigter Schneckenförderer*. Dissertation, Technische Universität München, 2012.

M. Scheffler. *Fördermittel und ihre Anwendung für Transport - Umschlag - Lagerung*. Fachbuchverlag, Leipzig, 1980.

C. Schein. *Zum kontinuierlichen Trennpressen biogener Feststoffe in Schneckengeometrien am Beispiel geschälter Rapssaat*. Dissertation, Universität Duisburg-Essen, 2003.

D. Schulze. *Pulver und Schüttgüter – Fließeigenschaften und Handhabung*. Springer Vieweg, Berlin Heidelberg, 2014. doi: 10.1007/978-3-642-53885-8.

M. Zlatev. *Beitrag zur quantitativen Kornformcharakterisierung unter besonderer Berücksichtigung der digitalen Bildaufnahmetechnik*. Dissertation, Technische Universität Bergakademie Freiberg, 2005.